ELSEVIER

Automation in Construction 16 (2007) 255 – 261

AUTOMATION IN CONSTRUCTION

www.elsevier.com/locate/autcon

Auto inspection system using a mobile robot for detecting concrete cracks in a tunnel

Seung-Nam Yu, Jae-Ho Jang, Chang-Soo Han *

Department of Mechanical Engineering, Hanyang University, Seoul, Korea

Accepted 8 May 2006

Abstract

To assess the safety of concrete structures, cracks are periodically measured and recorded by inspectors who observe cracks with their naked eye. However, manual inspection is slow and yields subjective results. Therefore, this study proposes a system for inspecting and measuring cracks in concrete structures to provide objective crack data to be used in evaluating safety. The system consists of a mobile robot system and a crack detection system. The mobile robot system is controlled to maintain a constant distance from walls while acquiring image data with a Charged Couple Device (CCD) camera. The crack detection system extracted crack information from the acquired image using image processing. To ensure accurate crack recognition, the geometric properties and patterns of cracks in a structure were applied to the image processing routine. The proposed system was verified with laboratory and field experiments.

Keywords: Crack; Tunnel; Inspection; Image processing; Mobile robot

1. Introduction

Approximately 70% of Korea consists of mountainous terrain necessitating the use of many tunnels for railroads and roads. A concern exists for the safety of concrete structures, such as tunnels, in traffic environments. To determine the safety of such structures, periodic inspections have been conducted using non-destructive tests. However, the slow and complicated procedures of the non-destructive tests prohibit the total replacement of visual inspection by humans. Therefore, non-destructive tests have been limited to precision inspections [1]. Visual inspection of concrete structures involves the measurement of cracks by inspectors walking along the surface of the structure while using only their naked eye. As such, the main disadvantage of visual inspection is that a rapid and complete survey cannot be ensured.

To solve these problems, various methods for automatic crack inspection using image processing have been developed. These methods have been applied in practical settings including roads, bridges, fatigues, and sewer-pipes [2–6].

The particular purpose of this study is to suggest an integrated system of a crack detection module and mobile robot for application to the tunnel environment.

Similar subjects have been studied and developed. Komatsu Engineering Corp. has developed and commercialized an image acquisition system that can acquire the images of road and tunnel linings by using a laser-scanning device. The Railway Technical Research Institute in Japan developed an image acquisition system for railway tunnel linings that uses line CCD (Charged Couple Device) cameras. Road ware Group Inc., based out of Canada, commercialized a system that acquires an image of the road at a speed of 80 km/h with a resolution of 3–4 cm. This system consists of a CCD camera, an ultrasonic sensor, and a gyro-sensor [7].

Such systems are useful for the collection of crack, leakage, scale, and spall image data; however, they do not provide automatic crack detection. An algorithm for crack detection and measurement must be developed to achieve a fully automatic inspection system, which is required for the rapid and objective assessment of crack data.

Cameras and lasers are used widely to obtain images for the inspection of structure surfaces. The cost of the laser-scanning device is prohibitive; additionally, it has a heat problem that affects system maintenance. Both attributes make it an inefficient

* Corresponding author. Tel.: +82 31 400 5247; fax: +82 31 406 6398.
E-mail address: cshan@hanyang.ac.kr (C.-S. Han).

0926-5805/$ - see front matter © 2006 Elsevier B.V. All rights reserved.
doi:10.1016/j.autcon.2006.05.003

Table 1
Matrix camera vs. line scan camera

	Matrix camera		L.S.C
Density	512×512	2000×2000	5000
Cost	Low	High	Low
No. of cam	20/10 m	5/10 m	2/10 m
Resolution	1 mm/pixel		

system for use in a wide array of fields. The camera-scanning device is more cost-effective than the laser device, but it has illumination problems in dark environments. Since cost is a major consideration for engineering implementations, surface image data acquisition must be studied further to achieve a low-cost camera acquisition method that ensures a high level of safety in concrete structures. In response to the aforementioned concerns, this study proposes to develop an automated surface crack inspection system for a tunnel that consists of a mobile robot and crack detection system. This would be faster, cheaper and more efficient than manual inspection.

2. Experiment condition

The mobile robot system, which was kept at a constant distance from the wall being inspected, acquires image data with a line CCD camera that scans the wall without the aid of inspectors. Table 1 refers to the comparison of two types of cameras and Table 2 shows the specification of the CCD camera used in this study.

To obtain fine grain images, the robot used a high power illuminator, shock absorbing devices, and a sensor that measures system velocity to control the line CCD camera. To achieve a resolution of 0.3 mm/pixel, the system can operate at up to 5 km/h.

The crack detection system consists of software that extracts the thickness, length, and orientation of cracks; these are important factors for the fundamental inspection of a structural surface. To test the proposed system, experiments were performed inside of buildings and road tunnels as shown in Fig. 1.

3. Description of the inspection robot system

3.1. Inspection

In consideration of safety, concrete structures are inspected for cracks, leakage, spall and other attributes; however, cracks are of particular concern, for they most significantly affect the state of the concrete [8].

Cracks in concrete structures arise from poor repair, contractions due to rapid temperature decreases, fluctuations between contractions and expansions from temperature changes, and extra loads from partial ground expansion.

Table 2
Specifications of the line scan camera

Elements	Specification
Density	4096 pixels
Max. Line Rate	23 kHZ
Interfaces	LVDS

LVDS: Low Voltage Differential Signaling.

Fig. 1. Tunnels (Kyunggi-do, South Korea).

Cracks can be classified as vertical, horizontal, shearing or complex. About 40% of cracks are vertical, 11% are horizontal and 30% are shearing, see Fig. 2. [9].

3.2. System configuration

The mobile robot system consisted of optical, mechanical, and data storage devices. These devices stored images of the surface of the concrete structure, maximized the contrast distribution of crack and non-crack areas, and minimized the noise while the system automatically moves parallel to the structure.

The crack detecting system was software that extracts and computes the numerical crack information from the image data. The software extracted the length, width and orientation of cracks. The crack detecting system provided information that

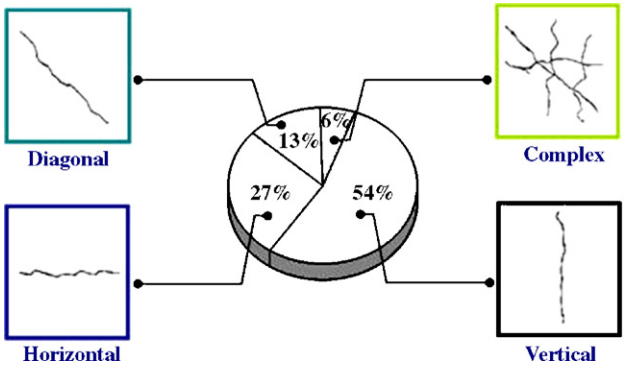

Fig. 2. Proportions of cracks.

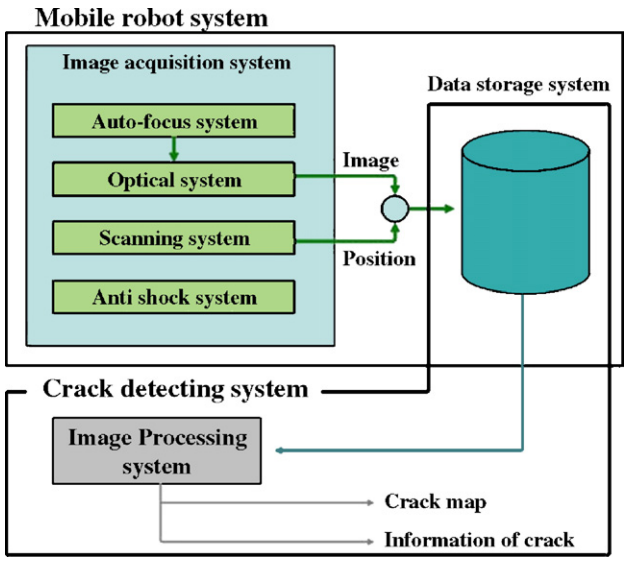

Fig. 3. Schematic diagram of integrated inspection system.

helps determine if additional precision inspection of a structure is needed.

The mobile robot system consisted of a CCD line camera, frame grabber, controlling apparatus for an auto-focus device, vibration-reducing device, illuminator and encoders to measure the velocity and position of the unit; this is shown in Fig. 3. To compute the distance of the robot from the structure, velocity and position were used, this allowed the camera to be focused and controlled without an inspector.

3.3. Mobile robot system

The robot has two wheels that are independently operated by two auto actuators. A diagram of the kinematical model resultant from the independent actuation of the wheels is shown in Fig. 4.

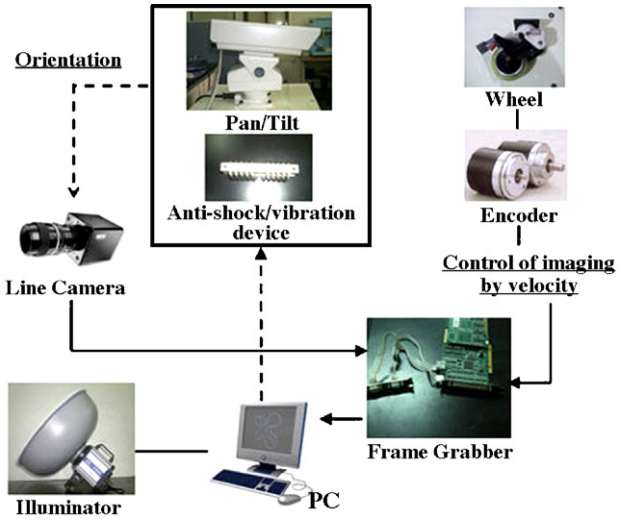

Fig. 4. Mobile robot system.

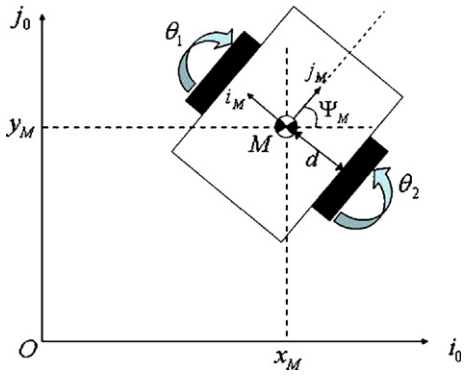

Fig. 5. Schematic diagram of mobile robot.

In Fig. 5 M is the standard point located at the center of gravity of the robot. O represents the origin point of the standard coordinate. It was assumed that the wheels of the robot could roll on a surface without sliding to the side. By making this assumption, the following kinematical formula was obtained.

$$\begin{aligned}\dot{x}_M &= \frac{r}{2}(\dot{\theta}_1+\dot{\theta}_2)\cos\Psi \\ \dot{y}_M &= \frac{r}{2}(\dot{\theta}_1+\dot{\theta}_2)\sin\Psi \\ \dot{\Psi}_M &= \frac{r}{2}(\dot{\theta}_1+\dot{\theta}_2)\end{aligned} \tag{1}$$

Eq. (1) is the kinematical function of the most generalized two-wheel driven robot. However, the first two formulas have a non-holonomic feature that cannot be completely integrated, making the robot difficult to control. The control point, or point where the wheels are connected to the robot, is separated from point M by a distance of d. When the control position is set in the middle of the robot, that is, when $d=0$, the control point cannot be accurately collected. However, when $d>0$, the control point is collected on 0. Therefore, d cannot be zero, but must be small enough to allow the control point to be set near to M.

This study used the main hardware and path tracking algorithm of the mobile system 'GSMR®' (Guided Service Mobile Robot),

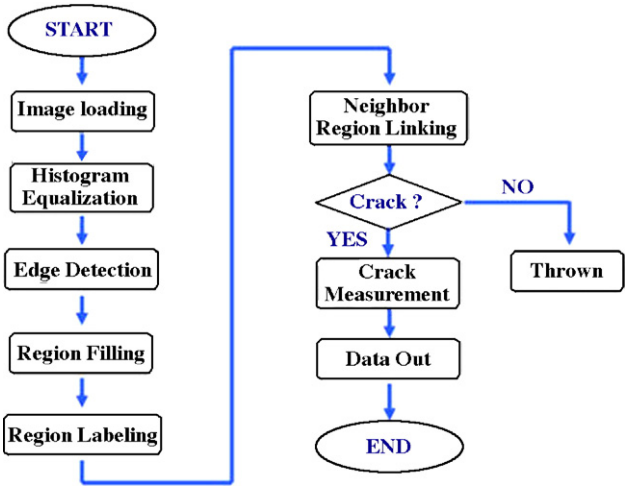

Fig. 6. Flowchart of the automatic inspection algorithm.

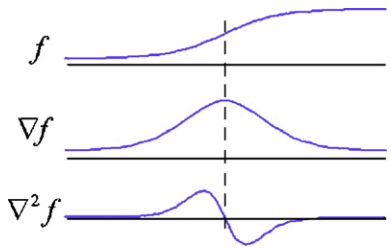

Fig. 7. 1D edge profile of the zero-crossing.

which was developed in 2002. More detail mathematical approaches are explained in Ref. [10].

4. Crack inspection algorithm

4.1. Theoretical approach

Cracks and non-crack areas are distinguished by their contrasting respective light reflectance values. The images derived from this pattern of reflection are assessed using a crack detection and physical measurement algorithm. Total automation by image processing is currently limited because accurate results are difficult to obtain in unpredictable environments. Thus, in this study, a semi-automatic algorithm for complete crack detection was realized using the Dijkstra method of Fig. 6.

Although the illuminator of the crack detection system was not completely stable, a high degree of contrast between crack and non-crack areas may be achieved by the equalization shown in Eq. (2).

$$S_k = \sum_{j=0}^{k} \frac{n_j}{n} \qquad k = 0, 1, 2, \ldots L-1 \tag{2}$$

Where,

s_k	Acquired normalized gray-level value
n	Number of pixels
n_j	Number of pixels that have j gray-level value
k	The input gray-level

Crack information was extracted from the images by applying the Sobel and Laplacian operators, which find crack edges. The Sobel operator obtains the orientation of the edge, as shown in Eq. (3) [11].

$$\phi = a\tan 2\left(\frac{\partial f}{\partial y}, \frac{\partial f}{\partial y}\right) \qquad f_G = f \otimes G \tag{3}$$

where

$$G = \frac{1}{\sqrt{2\pi}\sigma} \exp\left(-\frac{x^2+y^2}{\sigma^2}\right)$$

It was easier to find the zero-crossing point from the second derivative than to find the maximum point from the first derivative, as shown in Fig. 7.

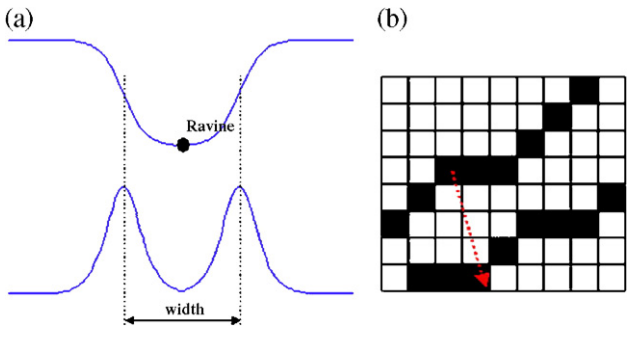

Fig. 8. Definition of detected edges. (a) 1D profile of ravine. (b) 2D profile of ravine.

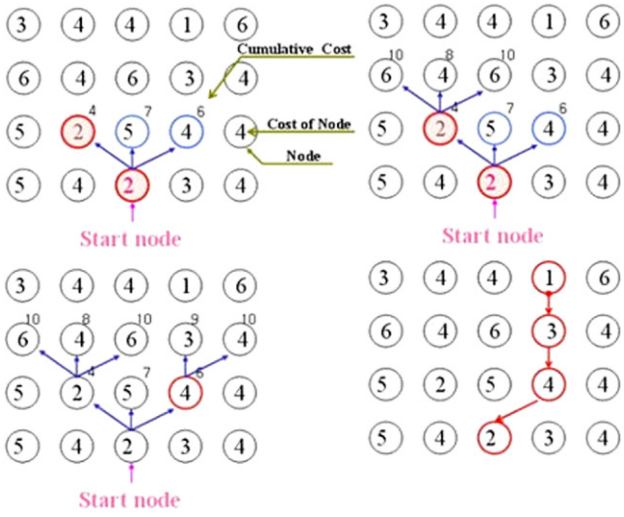

Fig. 9. Example of Dijkstra method.

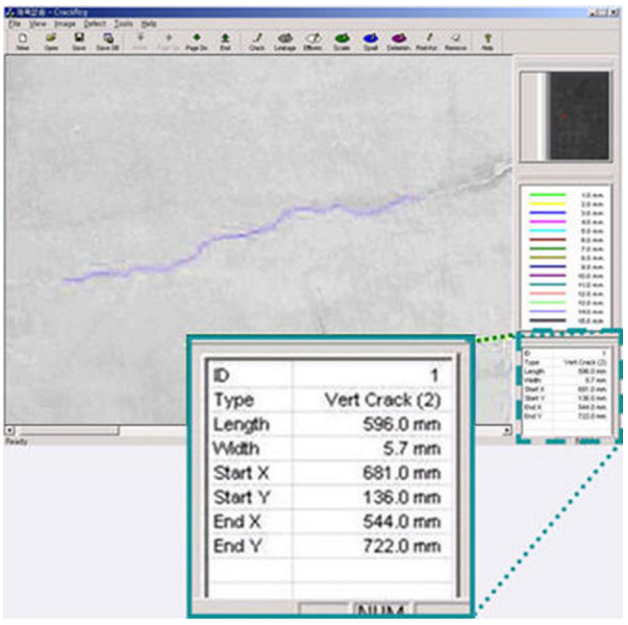

Fig. 10. Measurement of the crack.

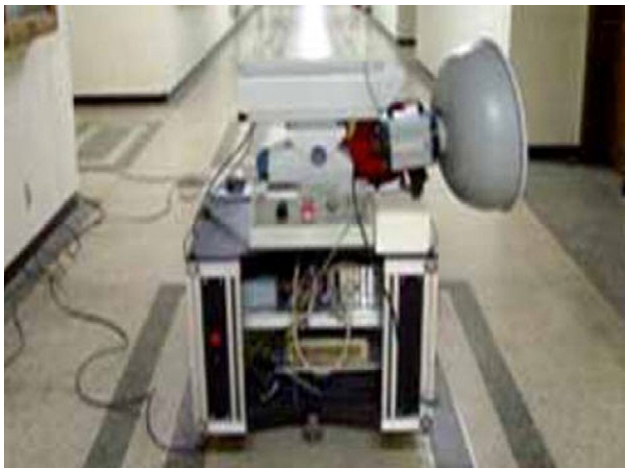

Fig. 11. Experimental setup in a building.

Additionally, the Laplacian operator is rotationally invariant, so the acquired edges were closed curve lines that were advantageous for targeting a region, including a crack edge.

As a second step, the stiff second derivative Gaussian filter was applied since the Laplacian operator is susceptible to noise.

The detected edges made a ravine, which was defined as a local minimum point between two edges, see Fig. 8. The 1D profile shown in Fig. 8(a) was generated by scanning the 2D image in the direction of the edges shown in Fig. 8(b).

Scanning from one crack edge to another was stopped when the following conditions were satisfied.

First, when another edge was crossed, the position of the local minimum point was acquired and stored. Then the width of the crack from its minimum point to its edge was calculated. Second, if the gray level of the current pixel was higher than that of any other edges, scanning was stopped. Finally, scanning was stopped when the scanned length was longer than a threshold value. The threshold value provided for a highly efficient calculation because it filtered noise, but cracks wider than the threshold value would be skipped.

Cracks extracted from images should be grouped according to their pattern of connection. In an image, a crack is a set of pixels.

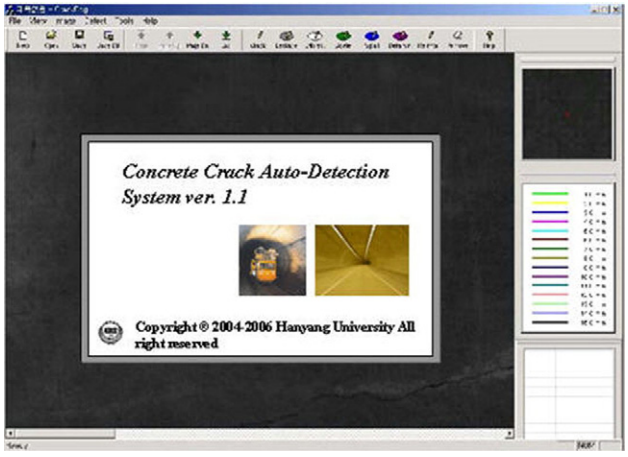

Fig. 12. Software of the crack detecting system.

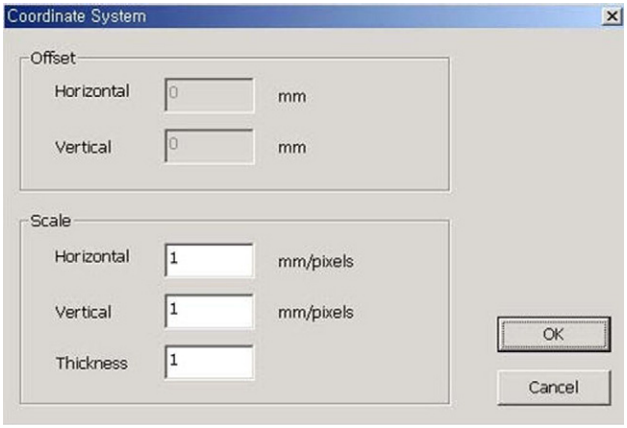

Fig. 13. Window for mapping data.

In this paper, the depth first search method was implemented to group and label each crack region [12]. Because the images were discontinuous, the connectivity between pixels may be low. This further influenced the calculation of features by sometimes inconsistently labeling cracks from the same region. To solve this problem, the slope of each segment end was computed with a certain number of pixels being modeled into a straight line. Segments were merged if the gradient change between them was miniscule.

4.2. Crack extraction via a graph search

With given start and end points, a graph was constructed by images and the boundary of the image was estimated through finding the least cost function. The pixels of an image were interpreted as nodes and eight-neighborhoods of a pixel were connected via links in the graph, using the Dijkstra method to find the shortest path [13].

Fig. 9 represents an example of Dijkstra Method.

The least cost function operated as follows.

Process 1 Input all nodes from the expansion of the start node into the queue. The previous node pointer is defined as nA. Then, calculate the cost of the expanded nodes.

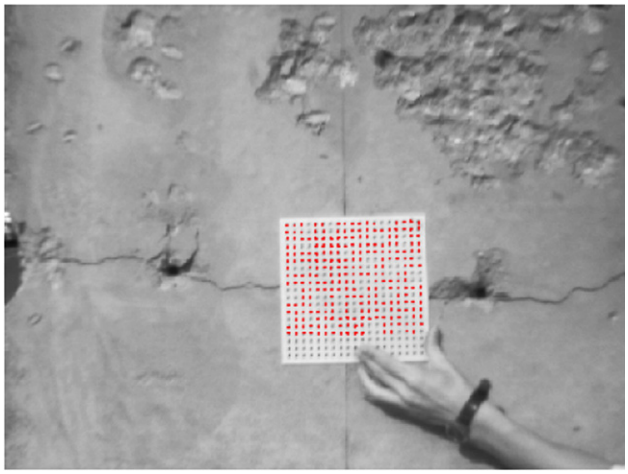

Fig. 14. Image overlay for calibration.

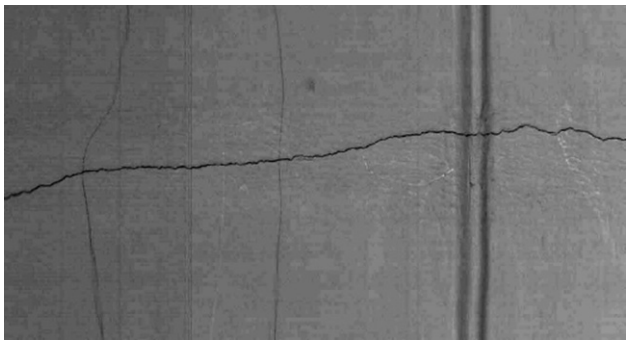

Fig. 15. Image of indoor wall.

Process 2 There is a failure if the queue is empty. Next, output the least cost node ni from the queue and remove it. If ni = nb, back-track the previous pointer saved in each node and terminates.

Process 3 If the condition to terminate in Process 2 was not satisfied, expand the node ni and input all other following nodes into the queue. Next, define the previous node pointer as ni and calculate each node cost. Go back to Process 2.

This algorithm always found an optimal value. However, numerous enlarged nodes may result from the function. To correct this inefficiency, a method that did not require the expansion of a node if the cost per unit length was above a certain value was used.

4.3. Crack measurement

Not all prospective cracks are actually cracks. Elements causing confusion include construction layers, an artificial mark, noise, or a blot. Potentially erroneous areas were removed when they were small enough to be considered noise, were not long and narrow, and were overly linear. Linear features are often construction layers or cables.

This paper used the quantum for the length, width, and direction of the crack. The widths of points composing each area were calculated when the region was formed from the edge. Outlier measurements were determined with the width derived as a mean value using five lengths of the median filter.

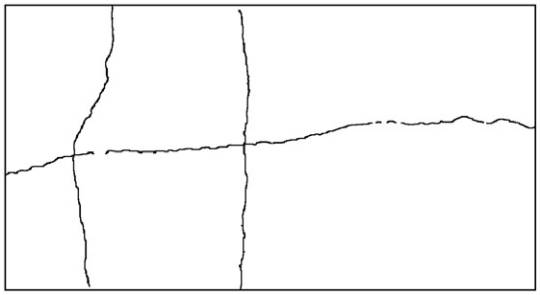

Fig. 16. Extracted crack of indoor wall.

Fig. 17. Image of subway inner wall.

This one extracts orderly middle value. The width of each area was calculated as in Eq. (4).

$$w = \frac{1}{N}\sum_{i=1}^{N} \hat{w}_i, \quad \hat{w}_j = \mathrm{med}\{w_{j-2},\ldots,w_{j+2}\} \tag{4}$$

N Number of areas
w mean value of width
$\hat{w}$ Median value of 5 lengths

The length of a crack was determined from the number of pixels in the image. After calculating the length of each diagonal as $\sqrt{2}$, and the vertical and horizontal lines as one, the real length was measured by camera calibration (Fig. 10).

5. Experiment

5.1. Experiment setup

An experiment was conducted in an indoor structure. A mobile robot with an encoder on its wheel obtained the image of the surface wall. The robot was capable of keeping a constant distance from the wall. If the mobile robot could not keep a constant distance from the wall, the image would remain in focus due to the use of an adjusting focus ring actuated by a laser distance sensor. To prevent vibration from being transmitted from the floor to the camera, the flat board holding the camera was stabilized with a wire rope. Fig. 11 shows the robot setup for indoor use.

Fig. 12 describes the image processing software. The crack information is shown on the right side of the software. Fig. 13 shows the menu for the camera calibration, the inputs were obtained by converting the distance between each pixel to millimeter. The camera was calibrated using a plate that had a

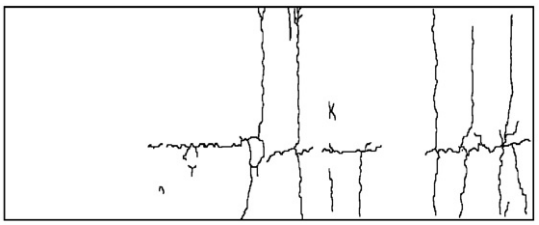

Fig. 18. Cracks extracted from the subway inner wall.

matrix of black dots on its surface; each separated by 5 mm. Fig. 14 shows an image overlay of both an obtained image and the extracted compensating points.

5.2. Experiment results

The image acquired from the indoor structure is shown in Fig. 15 and the detected cracks are shown in Fig. 16. The two vertical lines shown to the right in Fig. 15 are grooves embedded in the structure. Thus, these highly straight lines were removed after their recognition. The result of the experiment showed that the straight lines on the right side of Fig. 15 were excluded because those lines were not cracks.

Figs. 17 and 18 show the image processed and the cracks extracted, respectively.

As the finishing lines of the iron bars were not longish, but instead formed certain areas, they were not recognized as cracks.

Results were depicted pictorially to allow for discrimination by the human eye. The cracks were displayed using their vertical, horizontal, and diagonal orientations, as well as their length, width, starting and ending points. The crack inspection system proposed in this paper, though dependent on the state of the operating environment, had an overall error rate of 75–85%. The measurement error of recognized cracks was 10% or less.

Fig. 19 represents the wall image of a subway inner side tunnel wall. Using our system, the image was extracted following the distinguished line segment of Fig. 20.

This result showed that the proposed system was able to recognize cracks even when they were not longish in shape obviously need to more experiment, included spall, halls, and so on.

6. Conclusion

This paper proposed a structure crack inspection system that used image processing to avoid common human detection errors, including crack misidentification, slow detection, subjectivity, and data management inefficiency. The system was validated in indoor experimental settings, including an indoor structure, a road tunnel, and a subway tunnel. Even with advanced detection methods, erroneous recognition of cracks and non-cracks prevails. Therefore, the system was semi-automated to allow for the discarding of erroneous points, which was ensured by using a graph search method where the user inputs the start and end points of each crack.

In order to achieve a practical and applicable system, further study of crack characteristics and a fully automated algorithm must be conducted. It is hoped that this paper will encourage such future research.

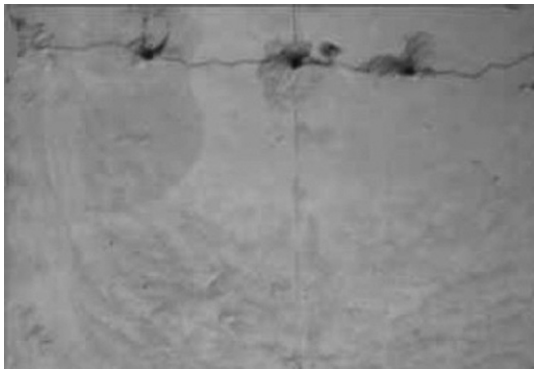

Fig. 19. Image of the subway inner wall including leakage, spall, and other forms of damage.

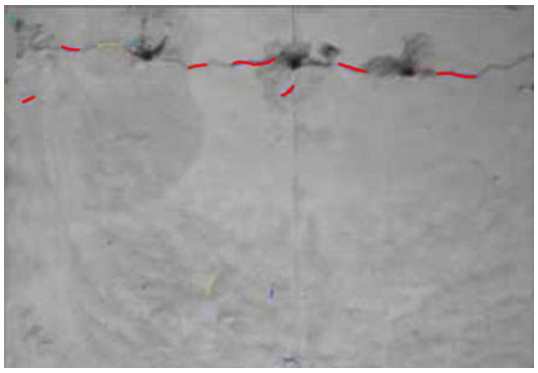

Fig. 20. Extracted image of the subway inner wall with cracks expressed by color according to width.

References

[1] Christian Huber, Habibollah Abiri, Stoyan I. Ganchev, Reza Zoughi, Analysis of the crack characteristic signal using a generalized scattering matrix representation, IEEE Transactions on Microwave Theory and Techniques 45 (1997).
[2] Sunil K. Sinha, Paul W. Fieguth, Automated detection of cracks in buried concrete pipe images, Automation in Construction 15 (January 2006) 58–72.
[3] Ikhlas Abdel-Qader, Osama Abudayyeh, M. ASCE, Michael E. Kelly, Analysis of edge-detection techniques for crack identification in bridges, Journal of Computing in Civil Engineering 17 (October 2003) 255–263.
[4] Pi-Cheng Tung, Yean-Ren Hwang, Ming-Chang Wu, The development of a mobile manipulator imaging system for bridge crack inspection, Automation in Construction 11 (October 2002) 717–729.
[5] Young-Suk Kim, Carl T. Haas, A model for automation of infrastructure maintenance using representational forms, Automation in Construction 10 (November 2000) 57–68.
[6] J. Pynn, A. Wright, R. Lodge, Automatic identification of cracks in road surfaces, image processing and its applications, Conference Publication, vol. 465, IEEE, 1999.
[7] Roadware Group incl.,http://www.roadware.ca.
[8] Developments of the safety assessment system and crack investigation equipment for tunnels (|), Report of The Korea Institute of Construction Technology, 1998.
[9] Evaluation and control of cracks in reingorced concrete structures, Report of The Ministry of Construction and Transpotation, Korea, 1996.
[10] Jae-Ho Jang, Tong-Jin Park, Chang-Soo Han, Development of a guide service mobile robot, ICCAS, 2002, pp. 2361–2366.
[11] A.K. Jain, Fundamentals of digital image processing, Prentice Hall Press, USA, 1989.
[12] R.E. Tarjan, Depth-first search and linear graph algorithms, SIAM Journal on Computing 1 (1972).
[13] Jayadev Misra, A walk over the shortest path: Dijkstra's algorithm viewed as fixed-point computation, Information Processing Letters 77 (2001).